HHS Public Access

Author manuscript

J Mol Cell Cardiol. Author manuscript; available in PMC 2021 February 01.

Published in final edited form as:

J Mol Cell Cardiol. 2020 February ; 139: 113–123. doi:10.1016/j.yjmcc.2020.01.008.

Location and Function of Transient Receptor Potential Canonical Channel 1 in Ventricular Myocytes

Qinghua Hu[a,c,*], **Azmi A. Ahmad**[a,b,*], **Thomas Seidel**[a], **Chris Hunter**[a], **Molly Streiff**[a,b], **Linda Nikolova**[d], **Kenneth W. Spitzer**[a], **Frank B. Sachse**[a,b]

[a]Nora Eccles Harrison Cardiovascular Research and Training Institute, University of Utah, Salt Lake City, UT 84112, USA

[b]Department of Biomedical Engineering, University of Utah, Salt Lake City, UT 84112, USA

[c]Department of Cardiothoracic Surgery, Xiangya Hospital, Central-South University, Changsha, Hunan, 410078, China

[d]Core Research Facilities, Health Sciences Center, University of Utah, Salt Lake City, UT 84112, USA

Abstract

Transient receptor potential canonical 1 (TRPC1) protein is abundantly expressed in cardiomyocytes. While TRPC1 is supposed to be critically involved in cardiac hypertrophy, its physiological role in cardiomyocytes is poorly understood. We investigated the subcellular location of TRPC1 and its contribution to Ca^{2+} signaling in mammalian ventricular myocytes. Immunolabeling, three-dimensional scanning confocal microscopy and quantitative colocalization analysis revealed an abundant intracellular location of TRPC1 in neonatal rat ventricular myocytes (NRVM) and adult rabbit ventricular myocytes. TRPC1 was colocalized with intracellular proteins including sarco/endoplasmic reticulum Ca^{2+} ATPase 2 in the sarcoplasmic reticulum (SR). Colocalization with wheat germ agglutinin, which labels the glycocalyx and thus marks the sarcolemma including the transverse tubular system, was low. Super-resolution and immunoelectron microscopy supported the intracellular location of TRPC1. We investigated Ca^{2+} signaling in NRVMs after adenoviral TRPC1 overexpression or silencing. In NRVMs bathed in Na^+ and Ca^{2+} free solution, TRPC1 overexpression and silencing was associated with a decreased and increased SR Ca^{2+} content, respectively. In isolated rabbit cardiomyocytes bathed in Na^+ and

Corresponding author: Dr. Frank B. Sachse, University of Utah, Nora Eccles Harrison Cardiovascular Research and Training Institute, 95 South 2000 East, Salt Lake City, UT 84112-5000, frank.sachse@utah.edu, Phone: 801-587-9514, Fax: 801-581-3128.

Author Contributions

Designed research: QH, AAA, KWS, FBS

Performed research: QH, AAA, MS, KWS, CH, LN

Analyzed data: QH, AAA, TS, MS, FBS

Wrote the manuscript: QH, AAA, MS, FBS

*contributed equally to this paper

Disclosures

None declared.

Ca^{2+} free solution, we found an increased decay of the cytosolic Ca^{2+} concentration $[Ca^{2+}]_i$ and increased SR Ca^{2+} content in the presence of the TRPC channel blocker SKF-96365. In a computational model of rabbit ventricular myocytes at physiological pacing rates, Ca^{2+} leak through SR TRPC channels increased the systolic and diastolic $[Ca^{2+}]_i$ with only minor effects on the action potential and SR Ca^{2+} content. Our studies suggest that TRPC1 channels are localized in the SR, and not present in the sarcolemma of ventricular myocytes. The studies provide evidence for a role of TRPC1 as a contributor to SR Ca^{2+} leak in cardiomyocytes, which was previously explained by ryanodine receptors only. We propose that the findings guide us to an understanding of TRPC1 channels as modulators of $[Ca^{2+}]_i$ and contractility in cardiomyocytes.

Keywords

TRPC1 channels; ventricular myocyte; sarcoplasmic reticulum; calcium signaling

Introduction

Transient receptor potential (TRP) channels were originally discovered in Drosophila [1]. Subsequently, a variety of TRP-related channels were identified in mammals. Based on homology of protein sequences TRP-related channels have been classified into seven families [2], including the family of transient receptor potential canonical (TRPC) channels that are expressed in the mammalian heart. While recent evidence suggests that TRPC channels are critical effectors in cardiac hypertrophy and heart failure [3–7], their physiological role in cardiac cells is still not understood [8]. Suggested roles for TRPC channels in these cells include store-operated and receptor-operated Ca^{2+} entry [9]. Store-operated Ca^{2+} entry is a mechanism by which the Ca^{2+}-depleted sarcoplasmic reticulum (SR) is refilled by Ca^{2+} flux through sarcolemmal ion channels into the cytosol and subsequent uptake in the SR. Receptor-operated Ca^{2+} entry is a mechanism by which Ca^{2+} flux through sarcolemmal ion channels is controlled by a receptor, commonly a G-protein-coupled receptor. In addition to a role in store-operated and receptor-operated Ca^{2+} entry TRPC channels in cardiomyocytes have been linked to mechano-electrical feedback, i.e. modulation of cellular electrophysiology by mechanical stimuli. This suggested role is based on studies indicating that some TRPC channels, including TRPC1 channels, are stretch-activated [10, 11].

A major obstacle to identification of a functional role of TRPC channels in cardiomyocytes is the diversity of information concerning subcellular location of the channels [8]. The location of TRPC channels in ventricular cardiomyocytes was primarily investigated in rodents. Several sarcolemmal locations were proposed: outer sarcolemma [12–14], transverse tubular system (t-system) [12–18], and sarcolemma at the intercalated disks [15]. Two types of sub-sarcolemmal location were suggested: subsarcolemmal vesicles and peripheral region of the myocytes [19, 20]. While a location of TRPC channels in intracellular membranes has been indicated in some studies [21, 22], the specific organelle was in general not specified. Interestingly, a study on skeletal muscle in rodent reported that TRPC1 resides in the SR [23]. This study suggested a functional role of TRPC1 channels in SR Ca^{2+} leak in skeletal myocytes.

Here, we shed light on the functional role of TRPC channels in ventricular cardiomyocytes. We focus on TRPC1, which is abundantly expressed in these cells. We tested the hypothesis that TRPC1 channels localized in the SR membrane of ventricular cardiomyocytes contribute to SR Ca^{2+} leak. In these cells, SR Ca^{2+} leak is commonly explained by ryanodine receptors (RyRs) [24].

First, we investigated the spatial distribution of TRPC1 in NRVMs. NRVMs allowed us to overexpress and silence TRPC1 expression using adenoviral TRPC1-eGFP and short hairpin (sh)RNA TRPC1-eGFP constructs, respectively. Importantly, NRVMs do not exhibit a t-system, which simplifies establishing a spatial relationship of TRPC1 to the sarcolemma. Next, we studied adult rabbit ventricular myocytes to relate findings from cultured neonatal cells to adult native cells with a t-system similar as in human ventricular myocytes. We performed three-dimensional (3D) confocal microscopy to visualize and reconstruct the distribution of TRPC1, sarcolemma, SR, and cytoskeletal proteins. We measured colocalization to investigate the spatial relationship of TRPC1 channels with the sarcolemma and various proteins. In addition, we applied super-resolution and immunoelectron microscopy to study the distribution of TRPC1 at nanometer scale. Subsequently, we used a cytosolic Ca^{2+} indicator and fluorescence microscopy in NRVMs to investigate if TRPC1 overexpression and silencing modulate SR Ca^{2+} leak. These studies were accompanied by studies on NRVMs and adult rabbit ventricular myocytes using a TRPC channel blocker. Finally, we applied a computational model of rabbit ventricular myocytes to explore a potential functional role of TRPC1 channels in electrophysiology and intracellular Ca^{2+} signaling.

Materials and Methods

All studies were conducted in accordance with National Institutes of Health Guidelines for the Care and Use of Animals and reviewed by the Institutional Animal Care and Use Committee at the University of Utah, where the work was performed. An additional Methods section is available in Supplementary Material.

Preparation, adenoviral infection and culture of NRVMs

Cells were enzymatically isolated from 1-day old rats (NCIS, Worthington Biochemical Corporation, Lakewood, NJ). NRVMs were subsequently separated from fibroblasts and plated at 175–200k density in 24 well tissue culture plates containing 5 mm coverslips treated with fibronectin. In some studies, NRVMs were then infected with an adenoviral vector containing a human TRPC1 attached to enhanced green fluorescent protein (TRPC1-eGFP) at 200 multiplication of infection (MOI) or eGFP (Cat No. 1060) as control at 25 MOI. In some studies, we also applied an adenoviral vector with human TRPC1 attached to enhanced green fluorescent protein and 6 HIS fused to the N-terminal. Furthermore, we infected NRVMs with shRNA TRPC1 with eGFP marker (shRNA-TRPC1-eGFP, Cat No. shADV-226536) to silence TRPC1 expression, or a scrambled RNA with eGFP marker (scRNA-eGFP, Cat No. 1122) as shRNA-TRPC1 control. Both infections were performed at 80 MOI. All viral vectors had a backbone of type 5 (dE1/E3), and were produced by Vector Biolabs (Malvern, PA). At 24 h after infection, cells were washed with DMEM to remove

the virus. Infected cells were then maintained and cultured for a total of 4–5 days by regularly exchanging the culture media, and incubating them in a humidity and CO_2 controlled incubator at 37 °C.

Immunolabeling of myocytes

NRVMs plated on coverslips were fixed for 15 min with 1% paraformaldehyde. Cells were permeabilized using 0.3% Triton X-100 (VWR International, Radnor, PA, USA) for 18 min and then bathed in image-iT FX Signal Enhancer (Thermo Fisher Scientific, Waltham, MA, USA) for 30 min and in 10% normal donkey serum (Millipore, Billerica, MA, USA) for 60 min. Cells were then incubated with primary antibodies for TRPC1 (T8666–09A, Supplementary Methods) and sarco/endoplasmic reticulum Ca^{2+} ATPase 2 (SERCA2) (MA3–910, Thermo Fisher Scientific) overnight at 4 °C. Subsequently, cells were incubated with secondary antibodies, a donkey anti-goat conjugated to Alexa Fluor 633 (Invitrogen, Carlsbad, California, USA) and a donkey anti-mouse conjugated to Alexa Fluor 555 for 60 min at room temperature. Finally, cells were incubated with DAPI (D3571, Thermo Fisher Scientific) for 15 min to stain nuclei. Cells were triple-rinsed with phosphate-buffered saline (PBS) for 15 min between each step.

Rabbit cardiomyocytes were isolated using enzymatic digestion (Supplementary Methods). Cell pellets were incubated with wheat germ agglutinin (WGA) conjugated to Alexa Fluor-633 for 20 min, followed by 15 min of fixation with 2% paraformaldehyde. Before applying primary antibodies, the cells were permeabilized using 0.1% Triton X-100 and blocked using 10% normal donkey serum. Commonly, two different primary antibodies were applied simultaneously, one raised in goat for labeling TRPC1 channels and the other raised in mouse for labeling other proteins. The cells were incubated with the primary antibodies overnight at 4°C. Two secondary antibodies, a donkey anti-goat antibody conjugated to Alexa Fluor 488 and a donkey anti-mouse antibody conjugated to Alexa Fluor 555, were then applied for 2 h at room temperature.

We assessed specificity of the TRPC1 antibody using confocal microscopy of skeletal muscle tissues from WT and TRPC1 knockout mice (Supplementary Methods and Fig. S1). Furthermore, we assessed our TRPC1 labeling protocol in rabbit cardiomyocytes by omission of the primary antibody and pre-incubation of the primary antibody with a blocking peptide, which both eliminated the TRPC1 signal (Fig. S2).

Confocal imaging and image processing

For acquiring 3D stacks of NRVMs, we used a Leica SP8 TCS microscope (Leica Microsystems, Wetzlar, Germany) equipped with GaAsP-HyD detectors and a 40x oil immersion lens (numerical aperture: 1.2). Alexa Fluor 488 was excited with a laser wavelength of 488 nm and emitted light was acquired after band-pass filtering from 491–555 nm. Alexa Fluor 555 and 633 were excited at 561 and 633 nm wavelengths, respectively. Fluorescence for excitation at 561 and 633 nm was collected at 566–604 and 638–775 nm, respectively. DAPI signal was excited with a 405 nm laser and collected at 410–570 nm.

For 3D imaging of segments of rabbit myocytes, we used a Zeiss LSM 5 Duo microscope (Carl Zeiss, Jena, Germany) equipped with a 63x oil immersion lens (numerical aperture:

1.4). Alexa Fluor 488 was excited with a 488 nm laser and emitted light was acquired after long pass filtering at 505 nm. Alexa Fluor 555 and Alexa Fluor 633 were excited at a wavelength of 543 nm and 633 nm, respectively. A 560 nm and 650 nm long pass filter was applied for light emitted from Alexa Fluor 555 and Alexa Fluor 633, respectively.

We acquired image stacks with a voxel size of 0.1 × 0.1 × 0.1 μm. The image stacks were preprocessed including noise reduction, deconvolution, background correction and attenuation correction as described previously [25]. We applied Pearson's correlation coefficient R_r to assess colocalization in the images (Supplementary Methods).

Measurement of $[Ca^{2+}]_i$ in myocytes

Experiments were conducted on NRVMs at 4–5 days post-infection. $[Ca^{2+}]_i$ was measured with a Leica SP8 TCS confocal microscope equipped with a 40x oil immersion lens (numerical aperture: 1.2) and GaAsP-HyD detectors. NRVMs were loaded with 10 μM Rhod-3 AM (R10145, Thermo-Fisher Scientific) in modified Tyrode solution at 37 °C for 45 min. After transfer into an imaging chamber, cells were superfused with the modified Tyrode solution at room temperature (22±1 °C). A 488 nm laser was applied to excite eGFP, and emitted light was collected after a 491–555 nm bandpass filter. A 561 nm laser was then used to excite Rhod-3 Ca^{2+} dye, and emitted light was collected using a 566 nm long pass filter. Na^+ and Ca^{2+} free Tyrode-like solution was used to block the sodium-calcium exchanger and other sarcolemmal Ca^{2+} currents.

Image sequences were acquired at a rate of 28 ms/image. Cells were initially paced by field stimulation at 0.5 Hz in modified Tyrode solution until reaching steady state Ca^{2+} signals. We then turned off the stimulation and rapidly switched to Na^+ and Ca^{2+} free solution for 2 minutes. Afterwards we rapidly applied 20 mM caffeine in the Na^+ and Ca^{2+} free solution to cause SR Ca^{2+} release and to estimate SR Ca^{2+} content as described previously [26]. The protocol was applied to NRVMs infected with eGFP, TRPC1-eGFP, shRNA-TRPC1-eGFP, and scRNA-eGFP. $[Ca^{2+}]_i$ transients were extracted from Rhod3 signal by cropping cytosolic regions with homogeneous intensities as described in Fig. S3. For analyses of SR Ca^{2+} content measurements, traces with multiple transients during the Na^+ and Ca^{2+} free period were excluded.

Similar studies on eGFP infected NRVMs were performed to assess RyR Ca^{2+} leak. SR Ca^{2+} content and leak were assessed with or without application of 1 mM tetracaine (Sigma-Aldrich) during the application of $Na^{\pm}$ and Ca^{2+} free solution. Furthermore, we carried out studies using the TRPC1-eGFP and eGFP constructs with or without application of 5 μM SKF-96365 (Sigma-Aldrich), a general TRPC channel blocker. SKF-96365 was dissolved in DMSO before adding it to Na^+ and Ca^{2+} free solution. Finally, we measured amplitudes of $[Ca^{2+}]_i$ transients from the various experiments using eGFP, TRPC1-eGFP, and shRNA-TRPC1-eGFP infected NRVMs.

Our protocol for measurement of $[Ca^{2+}]_i$ in rabbit ventricular myocytes is described in supplemental material. We applied SKF-96365 at a concentration of 5 μM as a non-specific blocker of TRPC channels [13].

Modeling of SR Ca^{2+} leak and effects on $[Ca^{2+}]_i$

Mathematical models of NRVMs and adult rabbit ventricular myocytes were used to shed light on effects of SR Ca^{2+} leak through TRPC1 channels on cellular electrophysiology and Ca^{2+} signaling for physiological pacing rates. We refer to the supplement for an introduction to our NRVM model. Our model of adult rabbit ventricular myocytes was based on a previously developed model [27], which comprises a description of passive SR Ca^{2+} leak into the junctional space through RyR channels. We added a description of Ca^{2+} fluxes through TRPC1 channels $J_{SR,TRPC}$ from the SR into the cytosol:

$$J_{SR,TRPC} = K_{SR,TRPC}\left(\left[Ca^{2+}\right]_{SR} - \left[Ca^{2+}\right]_i\right)$$

with the rate of leak $K_{SR,TRPC}$ and the SR Ca^{2+} concentration $[Ca^{2+}]_{SR}$. The rate $K_{SR,TRPC}$ was determined by fitting of self-ratioed cytosolic Ca^{2+} signals measured in the presence and absence of SKF-96365 to self-ratioed $[Ca^{2+}]_i$ calculated with the myocyte model. Simulations with the model were carried out using JSim (version 2.13) [28]. Simulation results after 1 min of pacing at 2, 3 and 4 Hz were analyzed for reduced, normal and increased Ca^{2+} fluxes through TRPC1 channels.

Statistical analysis

Data are presented as mean±standard error. Statistical analyses were performed in Matlab version R2012b and higher (Mathworks Inc., Natick, MA, USA). Comparison of experimental data was performed using a one-way analysis of variables (ANOVA). Comparison of data from epifluorescence microscopy was based on the paired student t-test. Differences were considered significant for P-values less than 0.01 or 0.05 where noted.

Results

Spatial distribution of TRPC1 in NRVMs

Applying confocal microscopy, we investigated the spatial distribution of wild-type (WT) TRPC1 in NRVMs that were cultured for 4–6 days, then fixed and labeled. Example sections from unprocessed and deconvolved 3D image stacks are presented in Fig. S4 and 1, respectively. Remarkably, TRPC1 exhibited a striated intracellular distribution (Fig. 1A). SERCA2 labeling presented a similar striated pattern, accompanied by an irregular network pattern spanning throughout the cell (Fig. 1B). The spatial distribution is particularly apparent in enlarged images (Fig. 1D and E). SERCA2 and TRPC1 appear to some degree colocalized in the overlay image (Fig. 1G).

After infection with TRPC1-eGFP constructs and culture of 4–5 days, NRVMs showed similar TRPC1 and SERCA2 patterns (Fig. 2A–D) as WT NRVMs (Fig. 1). Unprocessed stacks are shown in Fig. S5. Fluorescence of eGFP confirmed adenoviral TRPC1 expression (Fig. 2E and F). Overlay images present a similar colocalization of TRPC1 and SERCA2 antibody associated fluorescence (Fig. 2G) as in WT NRVMs, but only weak colocalization of TRPC1 and TRPC1-eGFP fluorescence (Fig. 2H) as well as partial colocalization of TRPC1-eGFP with SERCA2 fluorescence (Fig. 2I).

WT NRVMs exhibited high colocalization of SERCA2 and TRPC1 (R_r=0.4±0.03, n_{cells}=5). Similarly, R_r values for TRPC1 colocalization with SERCA2 across eGFP, TRPC1-eGFP, and shRNA-TRPC1-eGFP infected NRVMs were 0.46±0.03 (n_{cells}=5), 0.41±0.03 (n_{cells}=5), and 0.47±0.03 (n_{cells}=5), respectively (Fig. 2J). Differences were not significant between the groups. Colocalization of eGFP signal with SERCA2 was higher for TRPC1-eGFP versus eGFP and shRNA-TRPC1-eGFP infected cells (0.41±0.04 versus 0.26±0.02 and 0.22±0.04, respectively $P<0.05$, n_{cells}=5) (Fig. 2K).

Example images from confocal microscopy of TRPC1 labelled NRVMs infected with eGFP (7 images, ~30 cells), TRPC1-eGFP (14 images, ~40 cells), shRNA-TRPC1-eGFP (10 images, ~25 cells) and scrambled RNA constructs (3 images, ~30 cells) are shown in Fig. S6. In shRNATRPC1-eGFP infected cells, TRPC1 signals were small and striations rare (Fig. S6C) suggesting silencing of TRPC1 expression.

We acquired super-resolution images of TRPC1 and SERCA2 in WT NRVMs using single molecule localization (Supplementary Methods). The NRVMs exhibited a striated arrangement of TRPC1 clusters of variable size (Fig. 3A). SERCA2 exhibited a similar pattern and was in part in close proximity to TRPC1 (Fig. 3B and C).

Spatial relationship of TRPC1, SERCA2 and cytoskeletal proteins in rabbit ventricular myocytes

We imaged rabbit ventricular myocytes labeled with WGA and TRPC1 antibodies. WGA served as a marker of the outer sarcolemma and t-system. Exemplary images from co-labeling of WGA and TRPC1 are presented in Fig. 4. TRPC1 exhibited a striated transversal distribution along Z-lines as indicated by the t-system. The striated distribution is particularly evident in 3D visualization of cell segments (Fig. 4E). The majority of signal for TRPC1 did not overlap with WGA signal, suggesting that TRPC1 is localized in an intracellular membrane.

We confirmed presence of TRPC1 in rabbit ventricular myocardium using RNA sequencing (Supplementary Material, Fig. S7 and [29]). TRPC1 mRNA expression was higher than expression of other TRPCs.

Similar as for NRVMs, we investigated whether TRPC1 is located in the SR of adult rabbit cardiomyocytes using SERCA2 as a marker (Fig. 5). SERCA2 labeling presented a lattice-like pattern including transverse components adjacent to the Z-lines and longitudinal components spanning throughout the whole cell (Fig. 5B), which is in agreement with previous studies [30]. Visual inspection of the overlay images indicates that a large portion of TRPC1 was colocalized with transverse components of SERCA2 (Fig. 5C and D).

It has been suggested that the cytoskeleton is a major modulator of localization and function of the TRPC channels [31, 32]. Thus, we characterized the spatial relationship between TRPC1 and cytoskeletal proteins using confocal microscopy (Fig. 5E–H). Major components of the cytoskeleton are actin filaments, microtubules, and intermediate filaments. We therefore investigated α-actinin, which is an established marker for the Z-lines of sarcomeres, and vinculin, which is abundantly expressed in the costamere and intercalated

disks and plays a role in anchoring actin filaments to integrins. We also investigated β-tubulin, one of the subunits forming the heterodimer tubulin of microtubules, and desmin, a type III intermediate filament located adjacent to Z-lines.

TRPC1 was highly colocalized with α-actinin (Fig. 5E) and desmin (Fig. 5F). Beta-tubulin indicated a predominantly longitudinal orientation of microtubules, and its overlap with TRPC1 signals was small (Fig. 5G). TRPC1 was colocalized with vinculin (Fig. 5H) to a similar degree as with SERCA2.

In addition to visual inspection, we assessed the colocalization of TRPC1, WGA, SERCA2A and proteins of the cytoskeleton by calculating Pearson's correlation coefficient R_r from 3D image stacks. Our results using image stacks from cell segments *($n_{cells}=48$)* showed high values of R_r for TRPC1 with sarcomeric α-actinin (0.647±0.033), indicating spatial adjacency (Fig. 5I). Values of R_r were moderate for TRPC1 with desmin, vinculin and SERCA2. Small values of R_r for TRPC1 with β-tubulin and WGA indicate remoteness of TRPC1 from microtubules and sarcolemma, respectively. The colocalization of WGA with TRPC1 was as small as with α-actinin, β-tubulin and desmin (Fig. 5J).

Immunoelectron microscopy of TRPC1 in rabbit ventricular myocytes

Using immunoelectron microscopy we imaged the distribution of TRPC1 at nanometer resolution (Supplementary Material, Fig. S8). TRPC1 was extensively marked adjacent to the Z-lines and along the sarcomeres, but only few markers were found elsewhere. The abundance of the TRPC1 labeling appeared higher in regions close (within 200 nm) to the Z-lines than elsewhere, which agreed with our findings from confocal microscopy. However, instead of the regular striated pattern observed in confocal microscopy, a clustered distribution of TRPC1 was found in electron microscopy. In our images from immunoelectron microscopy TRPC1 was not visible in the t-system (Fig. S8A) and outer sarcolemma (Fig. S8B), supporting the idea that TRPC1 is located within the myocyte. Omission of primary antibodies served as negative control (Fig. S9).

Measurement of SR Ca^{2+} content in NRVMs

Our studies on TRPC1 location in NRVMs suggested that the channels are not in the sarcolemma, but in an organelle. Using confocal imaging and a Ca^{2+} sensitive dye we investigated SR Ca^{2+} content in NRVMs infected with eGFP, TRPC1-eGFP and shRNA-TRPC1-eGFP constructs (Fig. 6A, B and C, respectively). The protocol involved pacing of NRVMs, followed by bathing of quiescent cells in Na^+ and Ca^{2+} free solution for 2 minutes, followed by rapid application of caffeine (Fig. S3). Rapid application of caffeine led to a sudden increase of the Ca^{2+} signal, which is explained by RyR channel opening and Ca^{2+} release from the SR into the cytosol. We evaluated the SR content by measuring the amplitude of caffeine-induced peaks (Fig. 7). The SR Ca^{2+} content was measured in NRVMs infected with either eGFP (Fig. 7A), TRPC1-eGFP (Fig. 7B) or shRNA-TRPC1-eGFP (Fig. 7C). SR Ca^{2+} content was smaller in NRVMs overexpressing TRPC1 (1.64±0.21, $n_{cells}=21$) than in NRVMs infected with eGFP (3.18±0.23, $n_{cells}=15$, $P<0.01$). In contrast, SR Ca^{2+} content was significantly higher in NRVMs expressing shRNA-TRPC1

(4.30±0.49, n_{cells}=12, P<0.05) than in NRVMs expressing TRPC1-eGFP or eGFP. Studies were done on at least 8 litters per group.

Next, we studied effects of the TRPC channel inhibitor SKF-96365 on infected NRVMs (Fig. S10). Application of SKF-96365 increased SR Ca^{2+} content in both TRPC1-eGFP (2.56±0.45, n_{cells}=11, P<0.05) and eGFP (2.92±0.43, n_{cells}=13, P<0.01) versus TRPC1-eGFP infected cells in the absence of SKF-96365. As in Fig. 7D, NRVMs overexpressing TRPC1-eGFP had reduced SR Ca^{2+} content compared to eGFP NRVMs (1.56±0.22, n_{cells}=17 vs. 2.5±0.24, n_{cells}=14, P<0.01). Studies were done on at least 5 litters per group.

To study possible effects of short-hairpin infection on NRVMs, we conducted similar measurements of SR Ca^{2+} content with a scrambled RNA vector to serve as a separate control for the shRNA-TRPC1-eGFP group (Fig. S11). The difference was not significant between eGFP and scRNA-eGFP cells, suggesting that effects of shRNA-TRPC1-eGFP are due to silencing of TRPC1 expression.

To assess RyR Ca^{2+} leak, we applied 1 mM tetracaine. Example traces with and without tetracaine application are shown in Fig. S12A and B, respectively. We found differences in SR Ca^{2+} content (Fig. S12C) and self-ratioed $[Ca^{2+}]_i$ at the end of 2-min rest period (Fig. S12D). Application of tetracaine increased SR Ca^{2+} content (3.96±0.29, n_{cells}=21 vs 2.82±0.28, n_{cells}=17, p<0.01). Self-ratioed $[Ca^{2+}]_i$ at the end of 2-min rest period decreased with tetracaine (0.92±0.04 vs 1.09±0.06, p<0.05).

Amplitudes of $[Ca^{2+}]_i$ transients in response to the 0.5 Hz pacing decreased in NRVMs infected with TRPC1-eGFP (1.72±0.09, n_{cells}=49) compared to eGFP (2.19±0.17, n_{cells}=34, P<0.05) and shRNA-TRPC1-eGFP (2.42±0.24, n_{cells}=14, P<0.01). Differences between eGFP and shRNATRPC1-eGFP infected cells were not significant.

Measurement of $[Ca^{2+}]_i$ and SR Ca^{2+} content in rabbit ventricular myocytes

Using epifluorescence microscopy and a Ca^{2+} sensitive dye, we evaluated the decay of $[Ca^{2+}]_i$ and the SR Ca^{2+} content in rabbit ventricular myocytes bathed in Na^+ and Ca^{2+} free solution in absence and presence of SKF-96365. We observed a slow decay of the Ca^{2+} signal in quiescent cells in the absence of SKF-96365 (Fig. 8A), which is commonly explained by SR uptake and sarcolemmal leak of cytosolic Ca^{2+}. Application of the SKF-96365 intensified the Ca^{2+} signal decay versus control (−14.8% vs. −9.4%, n_{cells}=9, P<0.05) (Fig. 8B and C). The SR Ca^{2+} content in the presence of SKF-96365 was slightly elevated (1.50±0.26 versus 1.76±0.26, +17.3%, n_{cells}=6, P<0.05) (Fig. 8D). Peak systolic Ca^{2+} signals during action potentials just before switching to Na^+ and Ca^{2+} free solution were similar in the control and SKF-96365 group (Fig. S13), indicating that the SR Ca^{2+} content was also similar at that time.

Modeling of SR Ca^{2+} leak and effects on $[Ca^{2+}]_i$ in NRVMs

A mathematical model of NRVM electrophysiology [33] was modified to qualitatively reproduce our measurements of SR Ca^{2+} content. Applying the protocol from our studies on NRVMs (Fig. 7A–C) and varying SR Ca^{2+} leak, the model revealed a negative relationship between SR Ca^{2+} leak and release. The model reproduced experimental differences (Fig.

7D) of caffeine induced $\Delta[Ca^{2+}]_i$ due to TRPC1 silencing with a 98% decrease in leak and due to TRPC1 overexpression with 331% leak (Fig. S14B–E). The model also qualitatively predicted the decrease of $[Ca^{2+}]_i$ amplitudes in TRPC1-eGFP infected versus eGFP and shRNA-TRPC1-eGFP NRVMs that we found in our experimental studies.

Modeling of SR Ca^{2+} leak and physiological effects on $[Ca^{2+}]_i$ in rabbit ventricular myocytes

We used computational modeling to shed light on the role of TRPC1 channels in electrophysiology and Ca^{2+} signaling of rabbit myocytes at physiological pacing rates. Measured cytosolic Ca^{2+} decay in quiescent rabbit ventricular myocytes in the presence of SKF-96365 (Fig. 8C) was reconstructed by setting $\mathbf{K}_{SR,TRPC}$ to -1.1×10^{-5}/ms (Fig. S15A and B). The faster $[Ca^{2+}]_i$ decay in the presence of SKF-96365 was accompanied by a slowed decay of $[Ca^{2+}]_{SR}$ (Fig. S15C and D). After two minutes decay, $[Ca^{2+}]_{SR}$ was elevated with SKF-96365 vs. control (at end of pacing: 0.52 mM, after 2 min: 0.50 mM vs. 0.48 mM, −4.0% vs% vs. −8.8%). The model predicts increased $[Ca^{2+}]_{SR}$ after SKF-96365 application (+5.2%), which is consistent with increased measured SR Ca^{2+} content (Fig. 8D).

We compared $[Ca^{2+}]_i$ transients in control cells, cells in presence of SKF-96365 and cells with increased expression of TRPC1 at pacing rates of 2, 3 and 4 Hz (Fig. 9A). We assumed that increased expression (or activation) of TRPC1 channels leads to an increase of SR Ca^{2+} leak to 400% versus control levels. Thus, effects of upregulated TRPC1 channels were reconstructed by increasing SR Ca^{2+} leak ($K_{SR,TRPC}$ =4.4×10^{-5}/ms).

For all cell models, minimal (diastolic) and maximal (systolic) $[Ca^{2+}]_i$ increased with increasing pacing rate (Fig. 9B and C). For all pacing rates, SR Ca^{2+} leak exhibited a positive relationship with extrema and the amplitude of the $[Ca^{2+}]_i$ transient. Modulation of the diastolic $[Ca^{2+}]_i$ was strongest (+23.1%) for high SR Ca^{2+} leak and low pacing rate. Modulation of the systolic $[Ca^{2+}]_i$ and amplitude was strongest (+7.4% and 3.3%, respectively) for high SR Ca^{2+} leak and high pacing rate.

Similarly, $[Ca^{2+}]_{SR}$ increased with pacing rates for all cell models (Fig. 9D). While SR Ca^{2+} leak exhibited a positive relationship with $[Ca^{2+}]_{SR}$ minima (Fig. 9E), the relationship with $[Ca^{2+}]_{SR}$ maxima was negative (Fig. 9F).

The effect of SR Ca^{2+} leak on action potentials was small (Fig. 9G and H). The action potential duration exhibited a negative relationship with pacing rate. Increased SR Ca^{2+} leak was associated with marginally increased action potential duration at 90% repolarization (APD_{90}) (Fig. 9I).

Discussion

Our studies provide insights into the subcellular location and functional role of TRPC1 in ventricular cardiomyocytes. Previous studies on cardiomyocytes suggested that TRPC1 are localized in the sarcolemma and involved in membrane electrophysiology and mechano-electrical coupling. Our studies using immunolabeling and confocal microscopy revealed an

intracellular distribution of TRPC1 in ventricular myocytes isolated from neonatal rat and adult rabbit hearts. TRPC1 was colocalized with SERCA2, an established marker of SR (Figs. 1, 2 and 5). Quantitative colocalization analysis based on Pearson's correlation coefficient calculated from 3D microscopic image stacks further supported intracellular expression of TRPC1 adjacent to Z-lines in adult rabbit myocytes. TRPC1 exhibited high colocalization with sarcomeric α-actinin, which is a marker of the Z-line (Figs. 5E and I). The degree of colocalization with WGA, an established marker of sarcolemma, was significantly lower (Figs. 4 and 5I) and comparable to colocalization of WGA with α-actinin, desmin and tubulin (Fig. 5J), which are cytoskeletal proteins not located in the sarcolemma. Due to limited spatial resolution of confocal microscopy, our approach cannot completely exclude sarcolemmal expression of TRPC1. To address this issue, we employed immunoelectron and super-resolution microscopy with a spatial resolution in the nanometer range. For NRVMs, super-resolution microscopy reproduced the striated intracellular pattern of TRPC1 in proximity to SERCA2 (Fig. 3) observed with confocal microscopy (Fig. 1). Electron microscopy of rabbit ventricular myocytes supported the absence of TRPC1 expression in the surface sarcolemma and t-system (Fig. S8). The images indicate a discrete intracellular distribution with partial clustering of TRPC1 adjacent to Z-lines. While our approach for immunoelectron microscopy did not identify the intracellular compartment where the TRPC1 reside, the majority of TRPC1 was found in or close to z-lines as well as within sarcomeres.

The SR membrane has a high density in the region of Z-lines in adult rat and sheep myocytes [34]. Accordingly, in our studies using confocal microscopy on adult rabbit ventricular myocytes we found an increased SERCA2 fluorescence associated with the Z-line. The colocalization of TRPC1 with SERCA2 and the striated pattern of TRPC1 support our hypothesis that TRPC1 is located in the SR membrane. We note that the cultured NRVMs used in our study do not exhibit a t-system, yet the striated organization of native TRPC1 (Fig. 1A) was similar to the TRPC1 organization in adult rabbit myocytes. Furthermore, regions of rabbit myocytes devoid of ttubules still showed a prominent TRPC1 signal (Fig. 4). This suggests that TRPC1 localization is independent of sarcolemmal organization.

To provide further evidence for a SR location of TRPC1 channels in ventricular myocytes, we investigated the relationship between TRPC1 expression and SR Ca^{2+} content in quiescent NRVMs held in Na^{+} and Ca^{2+} free solution for 2 min. SR Ca^{2+} leak was assessed by measuring SR Ca^{2+} content. We found that TRPC1 expression exhibited a negative relationship with SR Ca^{2+} content: expression of TRPC1-eGFP construct decreased the SR Ca^{2+} content in NRVMs, while silencing of TRPC1 with shRNA-TRPC1-eGFP increased SR Ca^{2+} content (Fig. 7). These results were qualitatively reproduced in a mathematical model with increased and decreased SR Ca^{2+} leak corresponding to TRPC1 upregulation and silencing, respectively (Fig. S14). Furthermore, application of 5 μM SKF-96365, an established blocker of TRPC channels, increased the SR Ca^{2+} content in TRPC1-eGFP infected NRVMs (Fig. S10). Since the experiments were performed in Ca^{2+}-free bathing solution and Ca^{2+} cannot enter the cells from the extracellular space, the source of increased $[Ca^{2+}]_i$ after caffeine application must be in intracellular pools. The action of SKF-96365 to increase SR Ca^{2+} content points at the SR as the intracellular Ca^{2+} pool, which supports our

imaging results. Blocking RyR leak with tetracaine (Fig. S12) led to similar increase in SR Ca^{2+} content as measured after silencing of TRPC1 using our shRNA-TRPC1-eGFP construct (Fig. S12C vs. 7D). Increased SR Ca^{2+} content was associated with a decrease in $[Ca^{2+}]_i$ at the end of the 2-min rest period (Fig. S12D). The similarity of effects of TRPC1 silencing and RyR block indicates that both localize to the same organelle. Collectively, these results suggest that TRPC1 channels contribute to Ca^{2+} leak from the SR into the cytosol.

Cultured NRVMS are in many aspects different than native ventricular myocytes, so we furthered our studies using adult rabbit ventricular myocytes. RNA sequencing suggested that TRPC1 is the most expressed member of the TRPC family in these cells (Fig. S7). Application of SKF-96365 increased the decay of $[Ca^{2+}]_i$ and the SR Ca^{2+} content in cells bathed in Na^+ and Ca^{2+} free solution (Fig. 8). As for NRVMs (Fig. S10), we explain this finding by block of TRPC1 channels in the SR and a subsequent reduction in SR Ca^{2+} leak.

Our studies provide evidence for the contribution of TRPC1 channels to Ca^{2+} leak from the SR into the cytosol in cardiomyocytes. SR Ca^{2+} leak in these cells has been explained by spontaneous sparks from RyRs, non-spark-mediated RyR leak and non-RyR leak [24, 26]. The contribution of spark-mediated to total leak is thought to be small at low SR Ca^{2+} concentration, but large for high SR Ca^{2+} concentrations. Non-RyR leak was suggested to amount to around 50% of the non-spark-mediated RyR leak. Knowledge on the structural basis of non-RyR leak is sparse. A 1,4,5-inositol-trisphosphate ($InsP_3$) dependent SR Ca^{2+} leak through $InsP_3$ receptors has been identified, but was found to be very low in the absence of $InsP_3$. Also, non-RyR leak was insensitive to block of the $InsP_3$ receptor. Based on our studies, we suggest that the enigmatic non-RyR leak is caused, at least in part, by fluxes through SR TRPC1 channels.

Our computational simulations using a mathematical model of rabbit ventricular myocytes with the addition of TRPC1 channels in the SR suggest that TRPC1 channels modulate Ca^{2+} transients at physiological pacing rates (Fig. 9). We assumed that TRPC1 channels allow Ca^{2+} to leak from the SR into the cytosol, which was described in a similar manner as Ca^{2+} leak through RyR channels already incorporated in this model. In our model, the leak was proportional to the difference between $[Ca^{2+}]_{SR}$ and $[Ca^{2+}]_i$, and thus dominated by $[Ca^{2+}]_{SR}$, which is approximately three orders of magnitude larger than $[Ca^{2+}]_i$. In the simulations we focused on sub-acute effects of TRPC1 channel activation at a similar time scale as in our experimental assessment of $[Ca^{2+}]_i$. Increased SR Ca^{2+} leak augmented $[Ca^{2+}]_i$ during all phases of action potentials at physiological pacing rates. In particular, diastolic and systolic $[Ca^{2+}]_i$ were increased by TRPC1 leak. Interestingly, effects of TRPC1 channels on action potentials were small with only marginal prolongation of APD_{90}. The prolongation is explained by increased $[Ca^{2+}]_i$ causing increased forward sodium-calcium exchanger activity, which is electrogenic. The prolongation also causes increased Ca^{2+} influx through L-type Ca^{2+} channels, which contributes to the increase of $[Ca^{2+}]_i$. Based on these simulations we propose a physiological role for TRPC1 channels in the SR of cardiac myocytes in modulation of $[Ca^{2+}]_i$ and thus contractility. In particular, the simulations suggest that leak Ca^{2+} through TRPC1 channels increases contractility in paced myocytes.

Our localization study on TRPC1 in NRVMs and rabbit ventricular myocytes is in conflict with previous studies on rodent cardiomyocytes, many of which used confocal microscopy [8]. It is, however, difficult to describe spatial relationships of the t-system and proteins in rodent using confocal microscopy. Compared to rabbit, the t-system in rodents is denser and tubules are of smaller diameter, which hinders investigations using confocal microscopy due to limitations of spatial resolution [35, 36]. To illustrate the issue, we imaged ventricular myocytes from adult rat using a similar experimental approach as for ventricular myocytes of rabbits (Supplementary Methods, Fig. S16). TRPC1 did not outline the outer sarcolemma. However, the dense t-system obscured localization of TRPC1.

Similar discrepancies regarding TRPC1 location emerged in studies of skeletal myocytes. In a study on mouse skeletal muscle, Gervasio et al. reported sarcolemmal expression of TRPC1 [37], whereas Stiber et al. described a sarcolemmal pattern of TRPC1 corresponding to costameres at the level of Z discs [38]. In contrast, Berbey et al. presented a striated pattern of TRPC1 that matched SERCA1 immunolabeling in mouse skeletal myocytes [23]. The study applied immunolabeling for endogenous TRPC1 and overexpressing TRPC1 conjugated with yellow fluorescent protein, which revealed an intracellular distribution of TRPC1 similar to our findings in cardiomyocytes.

Previous studies on oocytes and CHO cells suggested that TRPC1 constitute stretch-activated ion channels [10], which is however still controversially discussed [39, 40]. Based on those studies a role in membrane electrophysiology and mechano-electrical coupling of myocytes was proposed. While our studies did not provide evidence for a direct role of TRPC1 in membrane electrophysiology, the studies shed new light on mechanisms by which TRPC1 may contribute to mechano-electrical coupling. The mechano-sensitivity of TRPC1 channels may contribute to stretch-modulated SR Ca^{2+} leak.

Another topic that we attempted to address in this study is the spatial relationship between TRPC1 and cytoskeleton in cardiomyocytes. The cytoskeleton plays a critical role in anchoring, trafficking and functionally regulating TRPC channels [31]. Also, Ca^{2+} influx through TRPC channels was suggested to be involved in rearrangement and remodeling of the cytoskeleton in many cell types [32]. Our confocal microscopic images revealed that TRPC1 is highly colocalized with sarcomeric α-actinin, and to some degree with desmin and vinculin along the Z-lines, whereas the distribution of TRPC1 appeared to be perpendicular to microtubules. Although the degree of functional colocalization with cytoskeletal proteins is unknown, we suggest that the intimate relationship with the sarcomeres allows TRPC1 channels to sense mechanical strain in the cell interior.

Our studies provide insights into the functional role of TRPC1, thus it is tempting to extrapolate our findings towards understanding the pathophysiological role of TRPC1 channels. It was suggested that TRPC1 channels are critical players in cardiac hypertrophy and heart failure [41]. Several studies indicated pathological up-regulation of TRPC1 [4, 42]. For example, hypertrophic agents such as endothelin-1 were found to increase TRPC1 expression to 410% in NRVMs. A simple prediction from our findings and reported pathological up-regulation of TRPCs is that increased Ca^{2+} leak from the SR into the cytosol causes sustained increased $[Ca^{2+}]_i$. Sustained increase of $[Ca^{2+}]_i$ has been implicated

previously in hypertrophic signaling in cardiac myocytes [43]. Recent studies indicate that TRPC channels are potential targets for treating heart failure [7] and cardiac dystrophy [44]. Based on our findings the mechanism of TRPC blockade as a way to treat cardiovascular disease would be explained by reduction of SR Ca^{2+} leak leading to normalization of $[Ca^{2+}]_i$, and inhibition of hypertrophic signaling.

Our interpretation of the presented studies assumes that TRPC1 forms channels that conduct Ca^{2+}. Extensive prior work revealed that TRPC1 forms heteromeric channels with other members of the TRPC, TRPP and TRPV families [39]. This suggests that modulation of TRPC1 expression as performed in our studies will, beyond modulation of the density of homomeric TRPC1 channels, modulate the density of heteromeric channels and contribution of TRPC1 to those channels. Recently, it was hypothesized that TRPC1 acts as regulatory subunit in heteromeric channel complexes [39]. Further studies will be required to understand effects of modulation of TRPC1 expression and interpret our findings in the context of this hypothesis.

Limitations of our approach include the spatial resolution of confocal microscopy [36]. Limited resolution exacerbates assessment of colocalization of proteins. Another limitation is related to our approach for immunoelectron microscopy, which did not provide direct information on SR membrane.

We note the high variability of results using NRVMs, which is, in part, explained by the variable degree of expression of adenoviral constructs. Even beyond variable expression of adenoviral constructs, we noticed large variability in our studies on NRVMs. For instance, eGFP expressing NRVMs exhibited a large variability of SR Ca^{2+} content. This explains why application of SKF-96365 in these cells did not yield statistically significant differences (Fig. S10). The high variability complicates testing of statistical hypotheses. For instance, a-priori power analysis based on preliminary studies on cells infected with eGFP with and without SKF-96365 application suggested that a large sample size (n~1000) is required for statements on statistically significant differences between the two groups.

High variability in NRVM phenotypes also limits accuracy of the mathematical model. The original model was constructed from experiments in various laboratories where culture conditions were presumably heterogeneous and different to the conditions in our laboratory. Notably, temperature differences between the model and our experiments restrict direct comparison. The original model was developed from measurements with NRVMs at 32°C, while our experiments were performed at room temperature (~22°C). We applied room temperature in order to control pacing rate of the cells, but temperature affects many cellular functions. Thus, the simulations served primarily for a qualitative comparison with our experimental findings. A general limitation of our models is related to modeling of caffeine effects. We limited our modeling of NRVMs to the initial phase of Ca^{2+} release (Fig. S14D) relevant for comparison with our measurements. Further work e.g. accounting for wash-in and out of caffeine will be necessary to accurately model the decay phase.

We also note differences of the spatial distribution on native TRPC1 and TRPC1-eGFP (Fig. 2H). We speculate that different time scales for expression and localization of the native

TRPC1 and TRPC1-eGFP explain the differences. A significant amount of the TRPC1-eGFP construct may be still trafficking to the sites, where the native TRPC1 resides. Nevertheless, similar R_r values for SERCA2 with native TRPC1 (Fig. 2J) and TRPC1-eGFP (Fig. 2K) construct suggest trafficking of the construct to SR regions. The TRPC1-eGFP vector comprises fused eGFP molecule yielding fluorescence upon expression of the TRPC1 protein (Fig. 6B). In contrast, the eGFP and shRNA-TRPC1-eGFP vectors comprise a non-fused eGFP yielding fluorescence upon successful infection of the cell. Images from living NRVMs infected with eGFP and shRNA-TRPC1-eGFP constructs indicate cytosolic and nuclear localization of the construct (Fig. 6A and C), likely due to intracellular diffusion of the small non-fused eGFP molecule.

We acknowledge limitations of our functional studies related to the absence of specific blockers or activators for TRPC1 channels. These limitations triggered our development and application of adenoviral TRPC1 overexpression and silencing in the presented studies on NRVMs. Nevertheless, in some studies we applied SKF-96365, which is an unspecific TRPC channel blocker, which also affects TRPV2, TRPM8 and voltage-gated calcium (Ca_v) 1–3 channels [45]. We accounted, in part, for the weak specificity of SKF-96365 with our experimental protocol. SKF-96365 was applied to myocytes after pacing and during rest for 2 min. The membrane voltage of myocytes at rest is close to the Nernst voltage for potassium and thus voltage gated channels such as Ca_V1–3 are closed and not involved in our measurements. Further insights into potential effects of unspecific action of SKF-96365 arise from our RNASeq data from rabbit ventricular myocardium. These data suggest that expression of TRPC1 is much higher than expression of TRPC 3, 4, 6 and 7 (Fig. S7) as well as TRPV2 and TRPM8 [29]. While we cannot fully exclude that SKF-96365 effects on these channels affect our measurements, we note that the results from application of SKF-96365 (Figs. 8D and S12) are consistent with results applying TRPC1 silencing (Fig. 7).

Supplementary Material

Refer to Web version on PubMed Central for supplementary material.

Acknowledgements

We acknowledge molecular biology support and expert advice on adenoviral expression of the TRPC1 constructs from Dr. Michael Sanguinetti. We thank Dr. Boris Martinac for providing us with the TRPC1 construct. We also thank Mr. Brett Milash for his help with the RNASeq data analysis. We appreciate the support of Dr. Kate Larson, who provided us with tissue samples from WT and TRPC1 KO mice.

Sources of Funding

We acknowledge funding by the Nora Eccles Treadwell Foundation and the National Heart, Lung and Blood Institute (R01HL094464 and R01HL132067).

Abbreviations

eGFP	enhanced green fluorescent protein
NRVM	neonatal rat ventricular myocytes
RyR	ryanodine receptor

SR	sarcoplasmic reticulum
sh	short hairpin
TRP	transient receptor potential
TRPC1	transient receptor potential canonical 1

References

[1]. Montell C, Rubin GM, Molecular characterization of the Drosophila trp locus: a putative integral membrane protein required for phototransduction, Neuron 2(4) (1989) 1313–23. [PubMed: 2516726]

[2]. Nilius B, Owsianik G, Voets T, Peters JA, Transient receptor potential cation channels in disease, Physiol. Rev 87(1) (2007) 165–217. [PubMed: 17237345]

[3]. Watanabe H, Murakami M, Ohba T, Ono K, Ito H, The pathological role of transient receptor potential channels in heart disease, Circ. J 73(3) (2009) 419–27. [PubMed: 19202304]

[4]. Seth M, Zhang ZS, Mao L, Graham V, Burch J, Stiber J, Tsiokas L, Winn M, Abramowitz J, Rockman HA, Birnbaumer L, Rosenberg P, TRPC1 channels are critical for hypertrophic signaling in the heart, Circ Res 105(10) (2009) 1023–30. [PubMed: 19797170]

[5]. Eder P, Molkentin JD, TRPC channels as effectors of cardiac hypertrophy, Circ Res 108(2) (2011) 265–72. [PubMed: 21252153]

[6]. Vennekens R, Emerging concepts for the role of TRP channels in the cardiovascular system, J. Physiol 589(Pt 7) (2011) 1527–34. [PubMed: 21173080]

[7]. Seo K, Rainer PP, Shalkey Hahn V, Lee DI, Jo SH, Andersen A, Liu T, Xu X, Willette RN, Lepore JJ, Marino JP Jr., Birnbaumer L, Schnackenberg CG, Kass DA, Combined TRPC3 and TRPC6 blockade by selective small-molecule or genetic deletion inhibits pathological cardiac hypertrophy, Proc Natl Acad Sci USA 111(4) (2014) 1551–6. [PubMed: 24453217]

[8]. Ahmad AA, Streiff M, Hunter C, Hu Q, Sachse FB, Physiological and pathophysiological role of transient receptor potential canonical channels in cardiac myocytes, Prog Biophys Mol Biol 130(Pt B) (2017) 254–263. [PubMed: 28629808]

[9]. Parekh AB, Putney JW Jr., Store-operated calcium channels, Physiol Rev 85(2) (2005) 757–810. [PubMed: 15788710]

[10]. Maroto R, Raso A, Wood TG, Kurosky A, Martinac B, Hamill OP, TRPC1 forms the stretch-activated cation channel in vertebrate cells, Nat Cell Biol 7(2) (2005) 179–85. [PubMed: 15665854]

[11]. Spassova MA, Hewavitharana T, Xu W, Soboloff J, Gill DL, A common mechanism underlies stretch activation and receptor activation of TRPC6 channels, Proc Natl Acad Sci U S A 103(44) (2006) 16586–91. [PubMed: 17056714]

[12]. Huang H, Wang W, Liu P, Jiang Y, Zhao Y, Wei H, Niu W, TRPC1 expression and distribution in rat hearts, Eur. J. Histochem 53(4) (2009) e26. [PubMed: 22073358]

[13]. Wu X, Eder P, Chang B, Molkentin JD, TRPC channels are necessary mediators of pathologic cardiac hypertrophy, Proc Natl Acad Sci USA 107(15) (2010) 7000–5. [PubMed: 20351294]

[14]. Jiang Y, Huang H, Liu P, Wei H, Zhao H, Feng Y, Wang W, Niu W, Expression and localization of TRPC proteins in rat ventricular myocytes at various developmental stages, Cell Tissue Res 355(1) (2014) 201–12. [PubMed: 24146259]

[15]. Goel M, Zuo CD, Sinkins WG, Schilling WP, TRPC3 channels colocalize with Na+/Ca2+ exchanger and Na+ pump in axial component of transverse-axial tubular system of rat ventricle, Am J Physiol Heart Circ Physiol 292(2) (2007) H874–83. [PubMed: 17012351]

[16]. Ward ML, Williams IA, Chu Y, Cooper PJ, Ju YK, Allen DG, Stretch-activated channels in the heart: contributions to length-dependence and to cardiomyopathy, Prog Biophys Mol Biol 97(2–3) (2008) 232–49. [PubMed: 18367238]

[17]. Dyachenko V, Husse B, Rueckschloss U, Isenberg G, Mechanical deformation of ventricular myocytes modulates both TRPC6 and Kir2.3 channels, Cell Calcium 45(1) (2009) 38–54. [PubMed: 18635261]

[18]. Mohl MC, Iismaa SE, Xiao XH, Friedrich O, Wagner S, Nikolova-Krstevski V, Wu J, Yu ZY, Feneley M, Fatkin D, Allen DG, Graham RM, Regulation of murine cardiac contractility by activation of alpha(1A)-adrenergic receptor-operated Ca(2+) entry, Cardiovasc Res 91(2) (2011) 310–9. [PubMed: 21546445]

[19]. Fauconnier J, Lanner JT, Sultan A, Zhang SJ, Katz A, Bruton JD, Westerblad H, Insulin potentiates TRPC3-mediated cation currents in normal but not in insulin-resistant mouse cardiomyocytes, Cardiovasc Res 73(2) (2007) 376–85. [PubMed: 17156765]

[20]. Kojima A, Kitagawa H, Omatsu-Kanbe M, Matsuura H, Nosaka S, Ca2+ paradox injury mediated through TRPC channels in mouse ventricular myocytes, Br J Pharmacol 161(8) (2010) 1734–50. [PubMed: 20718730]

[21]. Eder P, Poteser M, Groschner K, TRPC3: a multifunctional, pore-forming signalling molecule, Handb. Exp. Pharmacol (179) (2007) 77–92. [PubMed: 17217051]

[22]. Kuwahara K, Wang Y, McAnally J, Richardson JA, Bassel-Duby R, Hill JA, Olson EN, TRPC6 fulfills a calcineurin signaling circuit during pathologic cardiac remodeling, J Clin Invest 116(12) (2006) 3114–26. [PubMed: 17099778]

[23]. Berbey C, Weiss N, Legrand C, Allard B, Transient receptor potential canonical type 1 (TRPC1) operates as a sarcoplasmic reticulum calcium leak channel in skeletal muscle, J Biol Chem 284(52) (2009) 36387–94. [PubMed: 19875453]

[24]. Bers DM, Cardiac sarcoplasmic reticulum calcium leak: basis and roles in cardiac dysfunction, Annu Rev Physiol 76 (2014) 107–27. [PubMed: 24245942]

[25]. Sachse FB, Torres NS, Savio-Galimberti E, Aiba T, Kass DA, Tomaselli GF, Bridge JH, Subcellular structures and function of myocytes impaired during heart failure are restored by cardiac resynchronization therapy, Circ. Res 110(4) (2012) 588–97. [PubMed: 22253411]

[26]. Shannon TR, Ginsburg KS, Bers DM, Quantitative assessment of the SR Ca2+ leak-load relationship, Circ Res 91(7) (2002) 594–600. [PubMed: 12364387]

[27]. Shannon TR, Wang F, Puglisi J, Weber C, Bers DM, A mathematical treatment of integrated Ca dynamics within the ventricular myocyte, Biophys. J 87(5) (2004) 3351–71. [PubMed: 15347581]

[28]. Butterworth E, Jardine BE, Raymond GM, Neal ML, Bassingthwaighte JB, JSim, an open-source modeling system for data analysis, F1000Res 2 (2013) 288. [PubMed: 24555116]

[29]. Streiff M, Ahmad AA, Hunter C, Sachse FB, Adult rabbit left ventricle RNAseq, Gene Expression Omnibus. Series Accession: GSE115605. ID: 200115605, 2018.

[30]. Isenberg G, Borschke B, Rueckschloss U, Ca2+ transients of cardiomyocytes from senescent mice peak late and decay slowly, Cell Calcium 34(3) (2003) 271–80. [PubMed: 12887974]

[31]. Smani T, Dionisio N, Lopez JJ, Berna-Erro A, Rosado JA, Cytoskeletal and scaffolding proteins as structural and functional determinants of TRP channels, Biochim. Biophys. Acta 1838(2) (2014) 658–64. [PubMed: 23333715]

[32]. Stiber JA, Tang Y, Li T, Rosenberg PB, Cytoskeletal regulation of TRPC channels in the cardiorenal system, Curr. Hypertens. Rep 14(6) (2012) 492–7. [PubMed: 23054893]

[33]. Korhonen T, Hanninen SL, Tavi P, Model of excitation-contraction coupling of rat neonatal ventricular myocytes, Biophys J 96(3) (2009) 1189–209. [PubMed: 19186154]

[34]. Pinali C, Bennett H, Davenport JB, Trafford AW, Kitmitto A, Three-dimensional reconstruction of cardiac sarcoplasmic reticulum reveals a continuous network linking transverse-tubules: this organization is perturbed in heart failure, Circ. Res 113(11) (2013) 1219–30. [PubMed: 24044951]

[35]. Soeller C, Cannell MB, Examination of the Transverse Tubular System in Living Cardiac Rat Myocytes by 2-Photon Microscopy and Digital Image-Processing Techniques, Circ Res 84(3) (1999) 266–275. [PubMed: 10024300]

[36]. Savio-Galimberti E, Frank J, Inoue M, Goldhaber JI, Cannell MB, Bridge JH, Sachse FB, Novel features of the rabbit transverse tubular system revealed by quantitative analysis of three-

dimensional reconstructions from confocal images, Biophys J 95(4) (2008) 2053–62. [PubMed: 18487298]

[37]. Gervasio OL, Whitehead NP, Yeung EW, Phillips WD, Allen DG, TRPC1 binds to caveolin-3 and is regulated by Src kinase - role in Duchenne muscular dystrophy, J. Cell Sci. 121(Pt 13) (2008) 2246–55. [PubMed: 18544631]

[38]. Stiber JA, Zhang ZS, Burch J, Eu JP, Zhang S, Truskey GA, Seth M, Yamaguchi N, Meissner G, Shah R, Worley PF, Williams RS, Rosenberg PB, Mice lacking Homer 1 exhibit a skeletal myopathy characterized by abnormal transient receptor potential channel activity, Mol. Cell. Biol 28(8) (2008) 2637–47. [PubMed: 18268005]

[39]. Dietrich A, Fahlbusch M, Gudermann T, Classical Transient Receptor Potential 1 (TRPC1): Channel or Channel Regulator?, Cells 3(4) (2014) 939–62. [PubMed: 25268281]

[40]. Gottlieb P, Folgering J, Maroto R, Raso A, Wood TG, Kurosky A, Bowman C, Bichet D, Patel A, Sachs F, Martinac B, Hamill OP, Honore E, Revisiting TRPC1 and TRPC6 mechanosensitivity, Pflugers Arch 455(6) (2008) 1097–103. [PubMed: 17957383]

[41]. Rowell J, Koitabashi N, Kass DA, TRP-ing up heart and vessels: canonical transient receptor potential channels and cardiovascular disease, J Cardiovasc Transl Res 3(5) (2010) 516–24. [PubMed: 20652467]

[42]. Ohba T, Watanabe H, Murakami M, Takahashi Y, Iino K, Kuromitsu S, Mori Y, Ono K, Iijima T, Ito H, Upregulation of TRPC1 in the development of cardiac hypertrophy, J Mol Cell Cardiol 42(3) (2007) 498–507. [PubMed: 17174323]

[43]. Houser SR, Molkentin JD, Does contractile Ca2+ control calcineurin-NFAT signaling and pathological hypertrophy in cardiac myocytes?, Sci Signal 1(25) (2008) pe31. [PubMed: 18577756]

[44]. Seo K, Rainer PP, Lee DI, Hao S, Bedja D, Birnbaumer L, Cingolani OH, Kass DA, Hyperactive adverse mechanical stress responses in dystrophic heart are coupled to transient receptor potential canonical 6 and blocked by cGMP-protein kinase G modulation, Circ Res 114(5) (2014) 823–32. [PubMed: 24449818]

[45]. Schaefer M, TRPs: modulation by drug-like compounds, Handb Exp Pharmacol 223 (2014) 1077–106. [PubMed: 24961981]

Highlights

- The physiological role of TRPC1 channels in cardiomyocytes is currently ill-defined
- TRPC1 channels are localized in the sarcoplasmic reticulum
- TRPC1 channels contribute to calcium leak from the sarcoplasmic reticulum
- Leak through TRPC1 channels affects calcium content in the sarcoplasmic reticulum

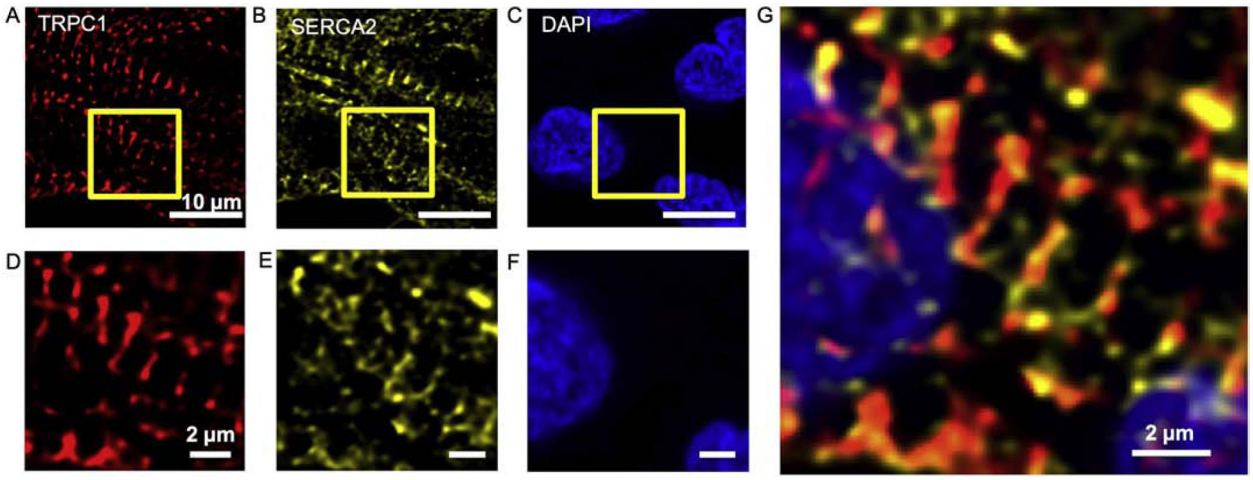

Figure 1.

Confocal microscopic images of fixed WT NRVMs labelled for TRPC1, SERCA2 and nuclei. The images were extracted from deconvolved 3D image stacks. (A) The spatial distribution of TRPC1 exhibits a striated pattern. (B) SERCA2, a marker for SR, presents a striated pattern accompanied with mesh-network pattern. (C) DAPI was used a marker for the nucleus. (D-F) Enlarged regions marked with box in (A-C), respectively. (G) Enlarged overlay of (D-F). Orange indicates overlap of TRPC1 and SERCA2 associated fluorescence. The scale bar in (A) applies to (B) and (C). Scale bar in (D) applies to (E) and (F).

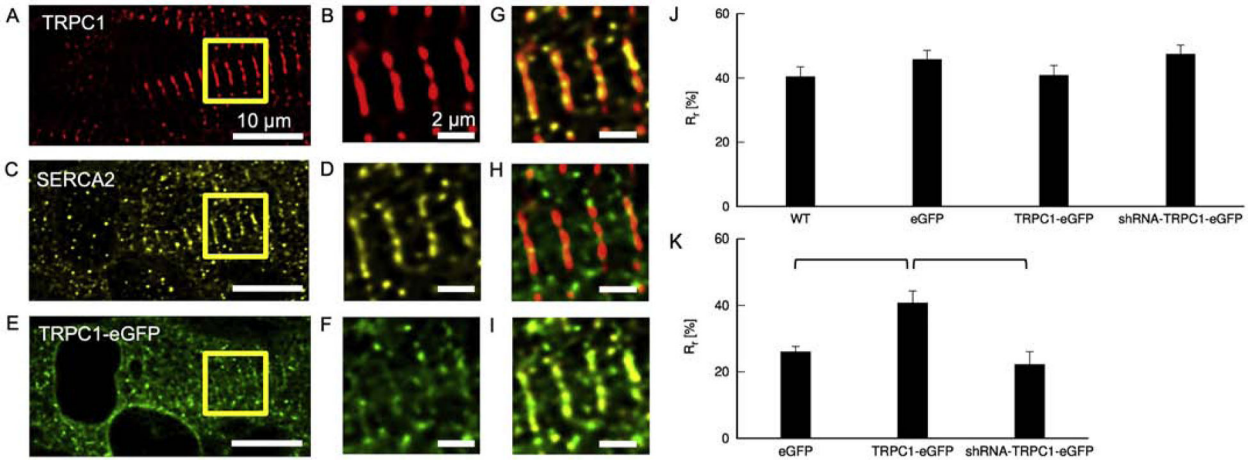

Figure 2.

Confocal microscopic images of fixed TRPC1-eGFP infected NRVMs and colocalization analyses. (A) Similar as in WT NRVMS, antibody labeling reveals a striated pattern of TRPC1. (B) Enlarged region marked with box in (A). (C) SERCA2 antibody indicating SR. (D) Enlarged region marked with box in (C). (E) Image of expressed TRPC1-eGFP construct. (F) Enlarged region marked with box in (E). (G) Overlay of (B) and (D). (H) Overlay of (B) and (F). (I) Overlay of (D) and (F). (J) Pearson correlation coefficient (R_r), calculated from image stacks of TRPC1 and SERCA antibody in different infection groups. (K) R_r calculated from image stacks of eGFP signal and SERCA antibody associated fluorescence in three infection groups. The scale bar in (A) applies to (C) and (E). Scale bar in (B) applies to (D), (F) and (G-I). Brackets mark significant differences ($P<0.05$)

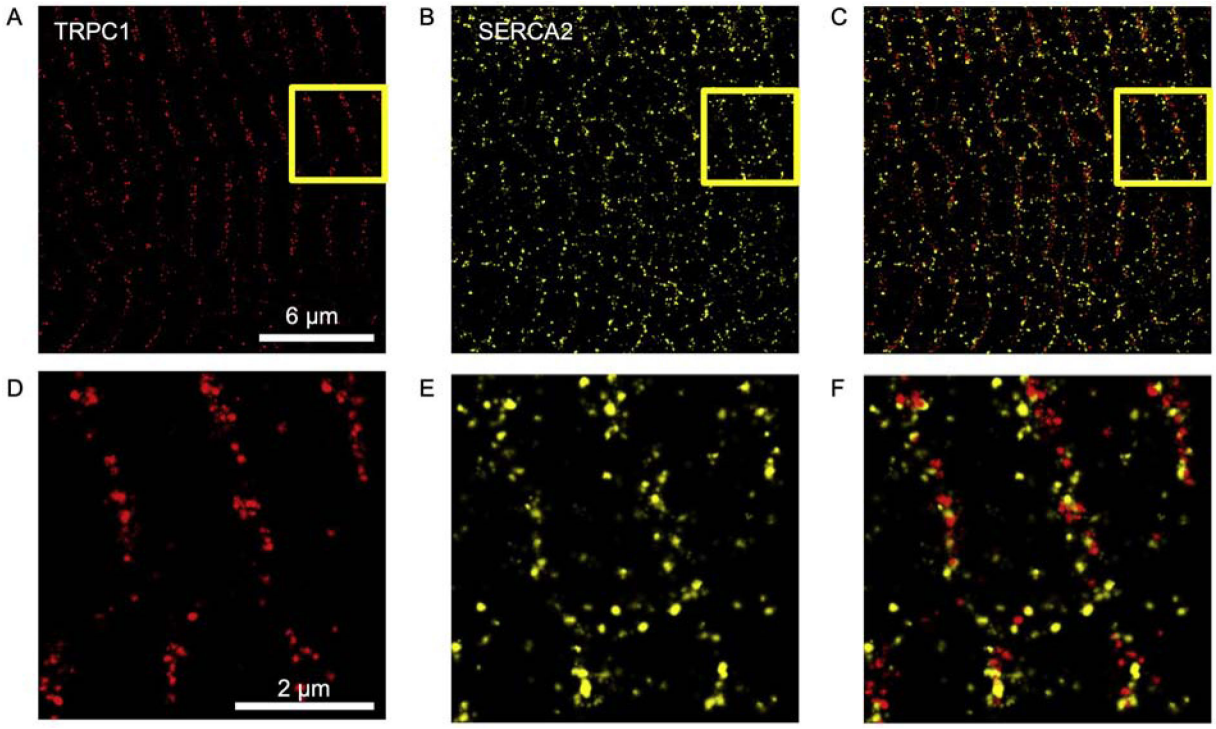

Figure 3.

Example super-resolution images of fixed WT NRVMs labeled with (A) TRPC1 and (B) SERCA2 antibody. (C) Overlay of images (A) and (B). (D-F) Enlarged regions marked by box in (A-C). TRPC1 and SERCA2 present a striated clustered arrangement. The scale bar in (A) applies to (B) and (C). Scale bar in (D) applies to (E) and (F).

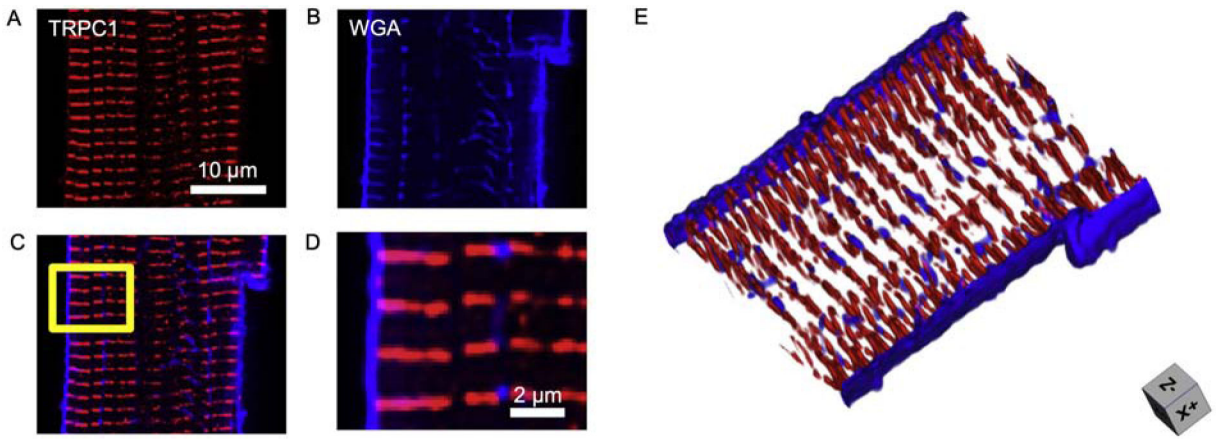

Figure 4.

Confocal microscopic images of TRPC1 and sarcolemma in adult rabbit ventricular myocyte. (A) TRPC1 exhibits a transversely striated distribution with the majority of TRPC1 within the cell. (B) WGA was used a marker for sarcolemma including t-system. (C) Overlay of (A) and (B). (D) Enlarged region marked with box in (C). (E) Three-dimensional visualization of cell segment.

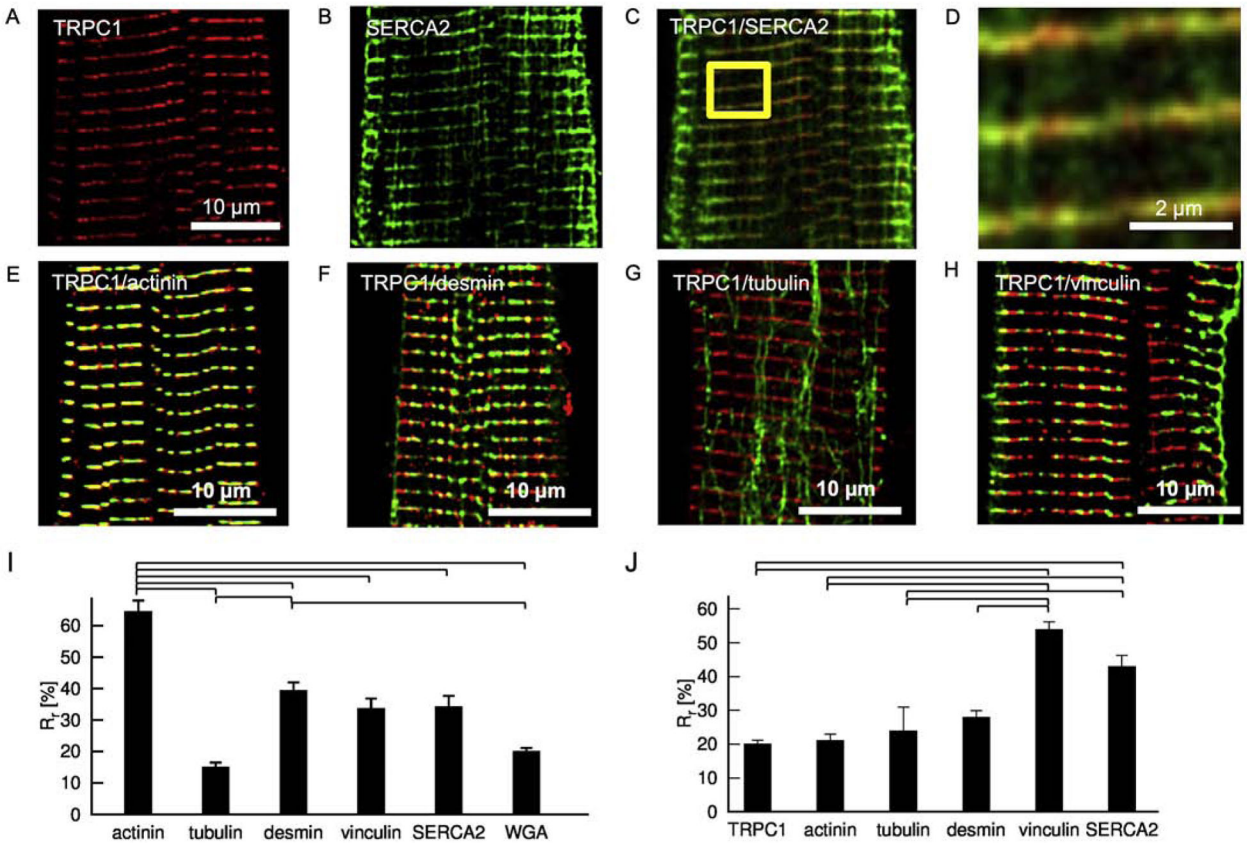

Figure 5.

Spatial distribution of TRPC1 in rabbit ventricular myocytes. Confocal microscopic images of (A) TRPC1 and (B) SERCA2. (C) Overlay of (A) and (B). (D) Enlarged region marked with box in (C). Yellow regions indicate colocalization of SERCA2 and TRPC1. The scale bar in (A) applies to (B) and (C). Confocal microscopic images of TRPC1 with (E) α-actinin, (F) desmin, (G) β-tubulin and (H) vinculin. (I) Pearson correlation coefficients (R_r) calculated from image stacks of TRPC1, intracellular proteins and WGA. (J) R_r determined from image stacks of WGA with TRPC1 and intracellular proteins. Brackets mark significant differences ($P<0.01$).

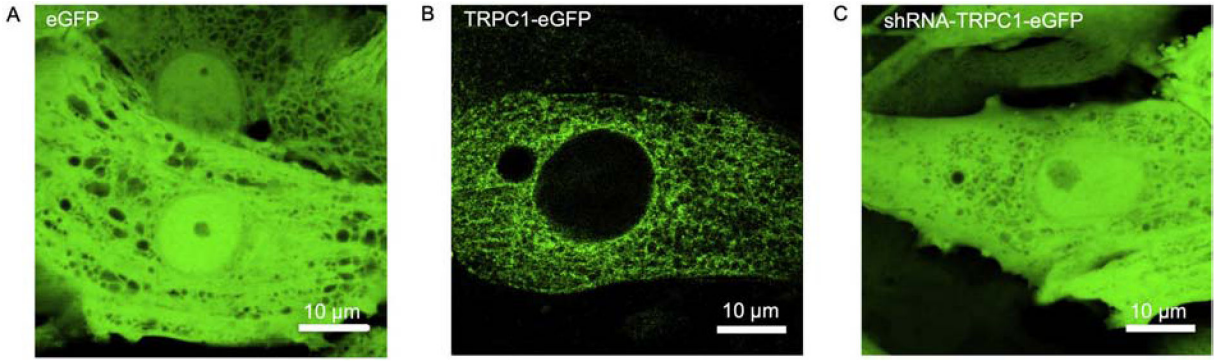

Figure 6.

Confocal microscopic images of living NRVMs infected with (A) eGFP at 25 MOI (B) TRPC1-eGFP at 200 MOI, and (C) shRNA-TRPC1-eGFP at 80 MOI.

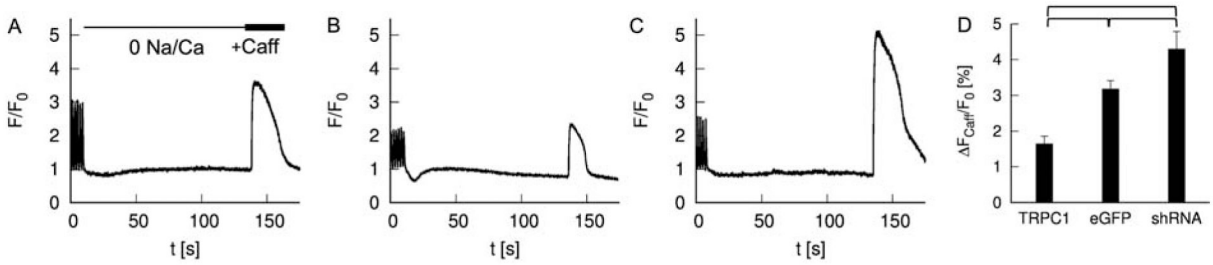

Figure 7.

Measurement and analysis of Ca^{2+} transients in NRVMs using confocal imaging. Self-ratioed Ca^{2+} signals (F/F_0) from a cell infected with (A) eGFP, (B) TRPC1-eGFP and (C) shRNATRPC1-eGFP constructs. SR Ca^{2+} content was assessed using rapid application of caffeine (20 mM). (D) Statistical analysis of SR Ca^{2+} release. Cells overexpressing TRPC1 and after silencing exhibited a decreased and increased amplitude of the self-ratioed Ca^{2+} signal $\Delta F_{Caff}/F_0$, respectively, versus control. Brackets mark significant differences ($P<0.05$).

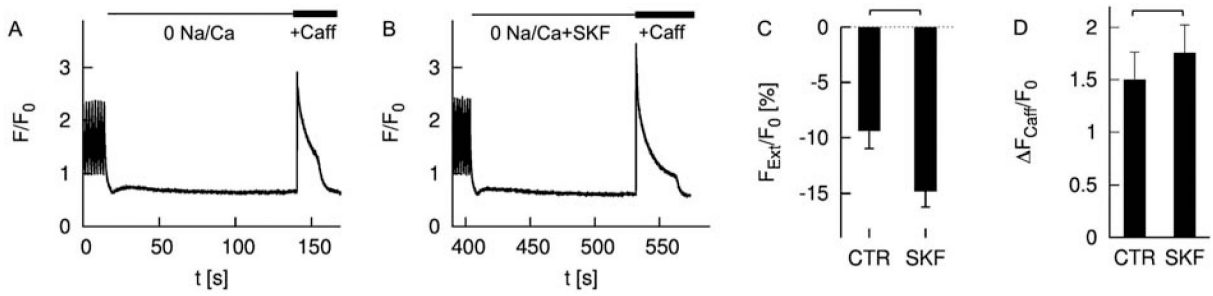

Figure 8.

Epifluorescence microscopy of rabbit myocyte using a cytosolic Ca^{2+} indicator. Self-ratioed Ca^{2+} signals (F/F_0) are presented for a cell undergoing pacing, followed by bathing with Na^+ and Ca^{2+} free solution (A) without and (B) with the TRPC channel blocker SKF-96365. In this cell, F/F_0 decreased in Na^+ and Ca^{2+} free solution. Subsequently, caffeine (20 mM) was rapidly applied. (C) Decay of F/F_0 after 2 min in Na^+ and Ca^{2+} free solution was increased in the presence of SKF-96365 (SKF) versus control (CTR). (D) Application of caffeine in cells bathed in SKF-96365 caused an increased amplitude of the self-ratioed Ca^{2+} signal $\Delta F_{Caff}/F_0$ versus control reflecting an increased SR Ca^{2+} content. Brackets mark significant differences ($P<0.05$).

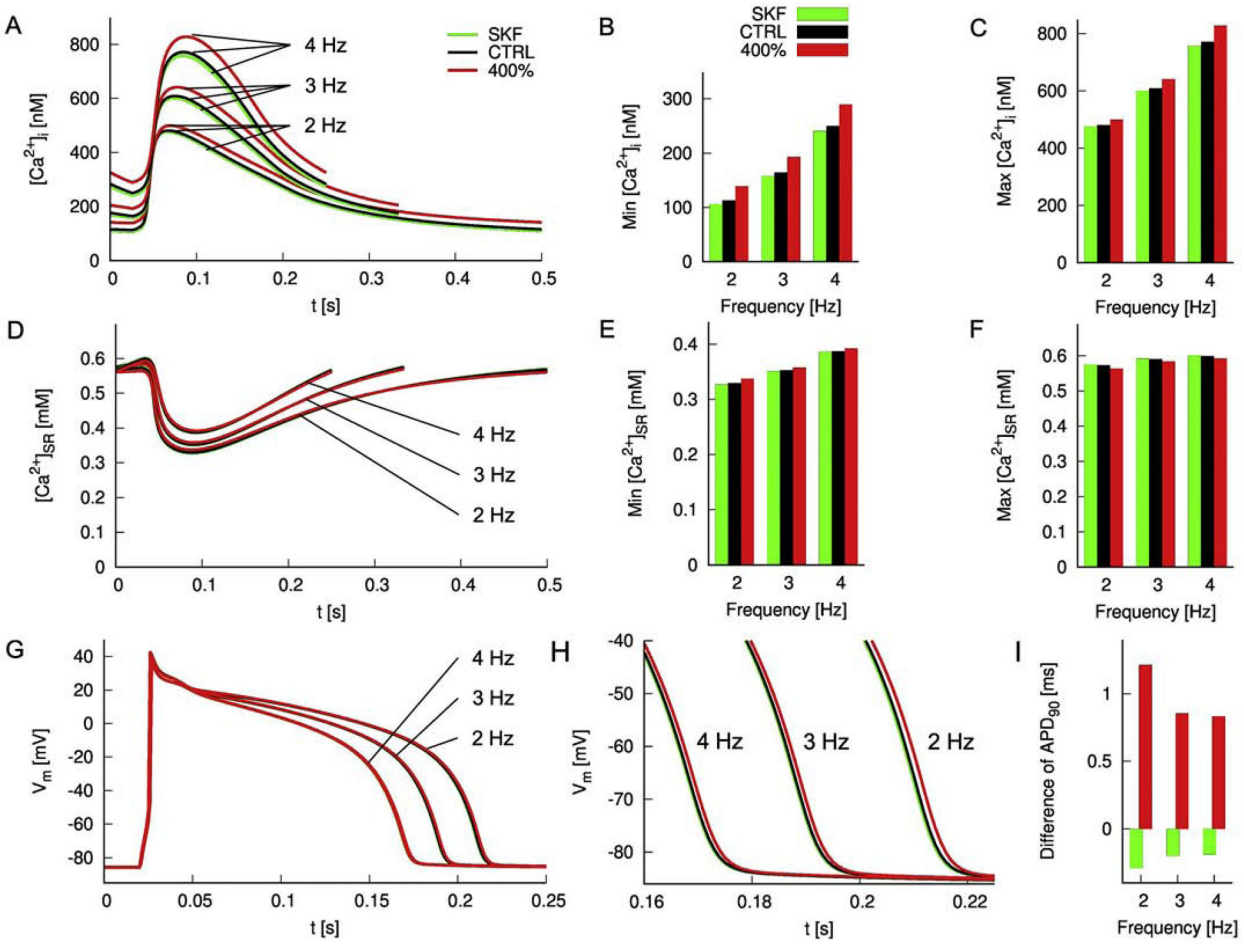

Figure 9.

Effects of SR Ca^{2+} leak current investigated in a computational model of rabbit ventricular myocytes. Simulations were performed at a pacing rate of 2, 3 and 4 Hz. Block (SKF-96365) and increased expression (400%) of TRPC1 channels were modeled by decreased and increased SR Ca^{2+} leak, respectively. (A) SR Ca^{2+} leak affected $[Ca^{2+}]_i$ at physiological pacing rates. In particular, SR Ca^{2+} leak exhibited a positive relationship with (B) minimal and (C) maximal $[Ca^{2+}]$. (D) $[Ca^{2+}i]_{SR}$ transients with associated (E) minima and (F) maxima. While SR Ca^{2+} leak exhibited a positive relationship with the minimal $[Ca^{2+}]_{SR}$, the relationship with maximal $[Ca^{2+}]_{SR}$ was negative. (G,H) SR Ca^{2+} leak had only a marginal effect on V_m. (I) In particular, variation of SR Ca^{2+} leak led to small differences of APD_{90} versus control.